

Towards nonlinear thermohydrodynamic simulations via the Onsager-Regularized Lattice Boltzmann Method

Anirudh Jonnalagadda,^{1,2,*} Amit Agrawal,³ Atul Sharma,³ Walter Rocchia,¹ and Sauro Succi^{4,2,5}

¹*Computational mOdeling of NanosCaLE and bioPhysical sysTEms (CONCEPT) Lab, Istituto Italiano di Tecnologia, 16152 Genova, Italy*

²*Center for Life Nano- & Neuro-Science, Fondazione Istituto Italiano di Tecnologia, Viale Regina Elena 295, Rome, 00161, Italy*

³*Department of Mechanical Engineering, Indian Institute of Technology Bombay, Mumbai 400076, India*

⁴*Istituto per le Applicazioni del Calcolo, Consiglio Nazionale delle Ricerche, Via dei Taurini 19, Rome, 00185, Italy*

⁵*Department of Physics, Harvard University, 17 Oxford St., Cambridge, 02138, MA, USA*

(Dated: January 28, 2025)

We present theoretical analyses of the recently proposed Onsager-Regularized (OReg) lattice Boltzmann (LB) method [Jonnalagadda *et al.*, *Phys. Rev. E* 104, 015313 (2021)] to demonstrate its ability to mitigate spurious errors associated with the insufficient isotropy of standard first-neighbor lattices without the inclusion of any external correction terms. As an illustration, we theoretically show that, with the so-called guided equilibrium, the OReg scheme inherently compensates for the insufficient lattice isotropy of the standard D2Q9 lattice by automatically adjusting the lattice viscosity; these theoretical results are verified numerically through simulations of the rotated decaying shear wave and isothermal shocktube problems. The present work lays the theoretical foundation of a generic framework which, with appropriately constrained equilibrium representations, can enable fully local, correction-free nonlinear thermohydrodynamic LB simulations on standard lattices, thereby facilitating scalable simulations of physically challenging fluid flows.

The evolution of a Lattice Boltzmann (LB) system [1–4] emulates the Boltzmann transport equation in D -dimensions through microscopic operations on discrete populations, f_i , in a lattice-discretized velocity space having N velocities $c_{i\alpha}$, $i \in \{1, \dots, N\}$. In such a discrete framework, the exact recovery of Navier-Stokes-Fourier (NSF) macrodynamics places explicit constraints on both the equilibrium and non-equilibrium contributions of f_i . Specifically, the discrete equilibrium state $f_i^{(eq)}$ is required to recover the Maxwell-Boltzmann (MB) moments:

$$\langle f_i^{(eq)}, \{1, c_{i\alpha}, c_i^2/2\} \rangle = \{\rho, \rho u_\alpha, E\} \quad (1a)$$

$$\Pi_{\alpha\beta}^{(eq)} = \Pi_{\alpha\beta}^{MB} = p\delta_{\alpha\beta} + \rho u_\alpha u_\beta \quad (1b)$$

$$q_\alpha^{(eq)} = q_\alpha^{MB} = u_\alpha(E + p) \quad (1c)$$

where the notation $\langle \varphi_i, \psi_i \rangle = \sum_i \varphi_i \psi_i$, ρ , ρu_α and $E = \Pi_{\alpha\alpha}^{(eq)}/2 = (Dp + \rho u^2)/2$ are the mass, momentum, and energy density respectively. $\Pi_{\alpha\beta}^{(eq)} = \langle f_i^{(eq)}, c_{i\alpha} c_{i\beta} \rangle$ and $q_\alpha^{(eq)} = \langle f_i^{(eq)}, \frac{c_i^2 c_{i\alpha}}{2} \rangle$ are the equilibrium contributions of the pressure tensor and heat flux vector, with pressure $p = \rho\theta$ where θ is the reduced temperature. Similarly, the non-equilibrium contributions of f_i must satisfy the so-called compatibility conditions (Eq. 2a) and should recover the NSF constitutive relations for the viscous stress tensor and heat flux vector (Eqs. (2b), (2c)),

$$\langle f_i^{(neq)}, \{1, c_{i\alpha}, c_i^2/2\} \rangle = 0, \quad (2a)$$

$$\Pi_{\alpha\beta}^{(neq)} = \Pi_{\alpha\beta}^{NSF} = -\mu \left(\partial_\alpha u_\beta + \partial_\beta u_\alpha - \frac{2}{D} \partial_\chi u_\chi \delta_{\alpha\beta} \right), \quad (2b)$$

$$q_\alpha^{(neq)} = q_\alpha^{NSF} = -\kappa \partial_\alpha \theta, \quad (2c)$$

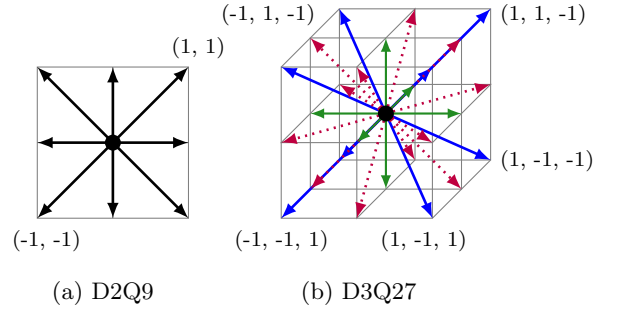


FIG. 1. Velocity space representations in two- and three-dimensions using the standard D2Q9 and D3Q27 lattices respectively.

where μ and κ are the dynamic viscosity and thermal conductivity respectively.

Eqs. (1a), (1b), and (1c), which correspond to 8 and 13 linearly independent constraints on the equilibrium distribution function in 2- and 3-dimensions, can be fully satisfied on standard lattices (Figure 1) lying within the first Brillouin zone through appropriate closed-form or numerical representations of $f_i^{(eq)}$. For the non-equilibrium populations, however, LB circumvents the need to have closed-form representations of $f_i^{(neq)}$ by, firstly, assuming that the compatibility conditions are satisfied on lattice stencils, and, secondly, evaluating the constitutive relations by coupling $\Pi_{\alpha\beta}^{(neq)} = \langle f_i^{(neq)}, c_{i\alpha} c_{i\beta} \rangle$ and $q_\alpha^{(neq)} = \langle f_i^{(neq)}, \frac{c_i^2 c_{i\alpha}}{2} \rangle$ to $f_i^{(eq)}$ via higher-order equilibrium moments $Q_{\alpha\beta\gamma}^{(eq)} = \langle f_i^{(eq)}, c_{i\alpha} c_{i\beta} c_{i\gamma} \rangle$ and $R_{\alpha\beta\gamma\mu}^{(eq)} = \langle f_i^{(eq)}, c_{i\alpha} c_{i\beta} c_{i\gamma} c_{i\mu} \rangle$.

However, this coupling to higher order equilibrium moments has significant repercussions in that spurious numerical errors are introduced on standard lattices due to

insufficient lattice isotropy. In order to retain the computational advantage provided by LB on standard lattices, significant efforts have been made over the past three decades to eliminate these spurious errors [5–17]. The current state-of-the-art incorporates non-local correction terms into the lattice update to exactly recover the desired thermohydrodynamics [12, 13, 16]. However, it is noteworthy that this strategy is not only hard to generalize to different collision kernels and equilibrium representations but is also detrimental to the parallel efficiency offered by LB on standard lattices. Furthermore, this performance sacrifice is exacerbated in numerical implementations that incorporate advanced meshing paradigms such as, e.g., grid refinement, needed for addressing complex problems involving fluid flow. In this work, we demonstrate, both theoretically and numerically, that the recently proposed Onsager-Regularized (OReg) LB method [18–20] facilitates simulations of non-linear hydro-thermal transport phenomenon by alleviating the adverse standard lattice anisotropy effects without resorting to non-local corrections.

The OReg scheme uses the principles of linear irreversible thermodynamics to obtain theoretically complete representations of $f_i^{(neq)}$. Noticeably, and in the spirit of the entropic LB which connects the discrete equilibrium and path length to kinetic theory via the discrete H-Theorem [21], the OReg formulation explicitly connects the description of the non-equilibrium lattice populations to kinetic theory via non-equilibrium thermodynamic descriptions. Indeed, using the OReg scheme Jonalagadda *et al.* [19] demonstrated a significant improvement in stability for flows with large Reynolds (Re) and Mach (Ma) numbers on standard lattices as compared to popular regularization strategies. We briefly revisit the OReg LB formulation in which the non-equilibrium contribution of the distribution function at the NSF level

is expressed in terms of viscous and thermal irreversible processes [22, 23] that comply with Onsager’s Symmetry Principle [24, 25]. We direct the interested reader to Ref. [19] for details and restrict ourselves only to the isothermal representation of the contribution of the continuous non-equilibrium populations corresponding to monatomic gases at the NSF order:

$$f^{(1)} = f^{\text{OReg}} = -\tau f^{\text{MB}} \left(C_\alpha C_\beta - \frac{C^2}{D} \delta_{\alpha\beta} \right) \left(\frac{\partial_\beta u_\alpha + \partial_\alpha u_\beta}{2\theta} \right). \quad (3)$$

Here, f^{MB} is the continuous Maxwell-Boltzmann equilibrium distribution function, $\tau = \frac{\mu}{p}$ is the relaxation time associated with the viscous irreversible process and $C_\alpha = (c_\alpha - u_\alpha)$ is the peculiar velocity. Note that Equation (3) can be recast into the same form [19] that is obtained from a Chapman-Enskog expansion of the continuous, force-free, integro-differential Boltzmann equation [26] and thus recovers the isothermal Navier-Stokes equations.

The OReg scheme directly projects Eq. (3) onto a lattice stencil by representing f^{MB} and C_α as $f_i^{(eq)}$ and $C_{i\alpha} = (c_{i\alpha} - u_\alpha)$, respectively. The hydrodynamic limit of the OReg scheme is obtained through a Chapman-Enskog multiscale expansion [27, 28] of the lattice-BGK equation:

$$f_i(x_\alpha + c_{i\alpha} \Delta t, t + \Delta t) - f_i(x_\alpha, t) = -\frac{1}{\tau} \left(f_i(x_\alpha, t) - f_i^{(eq)}(x_\alpha, t) \right), \quad (4)$$

where the distribution function is expressed as $f_i = f_i^{(0)} + \epsilon f_i^{\text{OReg}} + \mathcal{O}(\epsilon^2)$ and the temporal and spatial derivatives are $\partial_t = \partial_t^{(0)} + \epsilon \partial_t^{(1)} + \mathcal{O}(\epsilon^2)$ and $\partial_\alpha = \epsilon \partial_\alpha^{(1)}$ respectively; the parameter ϵ is a perturbation parameter corresponding to the Knudsen number. Explicitly, the $\mathcal{O}(\epsilon^3)$ mass and momentum conservation equations are recovered as:

$$\partial_t \rho + \partial_\alpha (\rho u_\alpha) = -\epsilon \left(\frac{1}{\tau} \langle f_i^{\text{OReg}}, 1 \rangle \right) - \epsilon^2 \left\{ \partial_t^{(1)} \left[\left(1 - \frac{\Delta t}{2\tau} \right) \langle f_i^{\text{OReg}}, 1 \rangle \right] + \partial_\alpha^{(1)} \left[\left(1 - \frac{\Delta t}{2\tau} \right) \langle f_i^{\text{OReg}}, c_{i\alpha} \rangle \right] \right\}, \quad (5a)$$

$$\partial_t (\rho u_\alpha) + \partial_\alpha (\Pi_{\alpha\beta}^{\text{MB}} + \Pi'_{\alpha\beta}) + \partial_\alpha [\epsilon \Pi_{\alpha\beta}^{(neq)}] = -\epsilon \left(\frac{1}{\tau} \langle f_i^{\text{OReg}}, c_{i\alpha} \rangle \right) - \epsilon^2 \partial_t^{(1)} \left[\left(1 - \frac{\Delta t}{2\tau} \right) \langle f_i^{\text{OReg}}, c_{i\alpha} \rangle \right], \quad (5b)$$

where $\Pi'_{\alpha\beta} = \Pi_{\alpha\beta}^{(eq)} - \Pi_{\alpha\beta}^{\text{MB}}$. Note that Eqs. (5a) and (5b) do not assume that the compatibility conditions

(Eq. (2a)) are satisfied. Instead, these quantities are explicitly evaluated for the OReg scheme to give:

$$\langle f_i^{\text{OReg}}, 1 \rangle = -\frac{\tau}{2\theta} \left(\partial_\beta^{(1)} u_\alpha + \partial_\alpha^{(1)} u_\beta \right) \left(\Pi'_{\alpha\beta} - \frac{\delta_{\alpha\beta}}{2D} \Pi'_{\chi\chi} \right) \quad (6a)$$

$$\langle f_i^{\text{OReg}}, c_{i\alpha} \rangle = -\frac{\tau}{2\theta} \left(\partial_\beta^{(1)} u_\alpha + \partial_\alpha^{(1)} u_\beta \right) \left[Q'_{\alpha\beta\gamma} - u_\alpha \Pi'_{\beta\gamma} - u_\beta \Pi'_{\gamma\alpha} - \frac{\delta_{\alpha\beta}}{D} \left(q'_\gamma - \frac{u_\gamma \delta_{\alpha\beta}}{2} \Pi'_{\chi\chi} \right) \right], \quad (6b)$$

where $Q'_{\alpha\beta\gamma} = Q_{\alpha\beta\gamma}^{(eq)} - Q_{\alpha\beta\gamma}^{\text{MB}}$ while $q'_\gamma = q_\gamma^{(eq)} - q_\gamma^{\text{MB}}$. Lastly, $\Pi_{\alpha\beta}^{(neq)}$ evaluated for the OReg scheme is:

$$\Pi_{\alpha\beta}^{\text{OReg}} = \left(1 - \frac{\Delta t}{2\tau}\right) \langle f_i^{\text{OReg}}, c_{i_\alpha} c_{i_\beta} \rangle = - \underbrace{\left[\left(\tau - \frac{\Delta t}{2}\right) \rho \theta \right]}_{\Pi_{\alpha\beta}^{\text{NSF}}} \left(\partial_\alpha u_\beta + \partial_\beta u_\alpha - \frac{2}{D} \partial_\chi u_\chi \delta_{\alpha\beta} \right) - \underbrace{\left(\tau - \frac{\Delta t}{2} \right) \frac{(\partial_\mu^{(1)} u_\gamma + \partial_\gamma^{(1)} u_\mu)}{2\theta} \left[R'_{\alpha\beta\gamma\mu} - u_\alpha Q'_{\beta\gamma\mu} - u_\beta Q'_{\alpha\gamma\mu} + u_\alpha u_\beta \Pi'_{\mu\gamma} - \frac{\delta_{\gamma\mu}}{D} (R'_{\alpha\beta\chi\chi} - 2Q'_{\alpha\beta\chi} + u_\chi^2 \Pi'_{\alpha\beta}) \right]}_{(\Pi_{\alpha\beta}^{(neq)})'}, \quad (7)$$

where, $R'_{\alpha\beta\gamma\mu} = R_{\alpha\beta\gamma\mu}^{(eq)} - R_{\alpha\beta\gamma\mu}^{\text{MB}}$ and $(\Pi_{\alpha\beta}^{(neq)})'$ is the error contribution in the NSF stress tensor. Here we highlight that, while Eqs. (6a), (6b) and (7) can be simplified depending on the constraints on $f_i^{(eq)}$, spurious contributions from $Q'_{\alpha\beta\gamma}$ and $R'_{\alpha\beta\gamma\mu}$ are still retained on standard lattices. Nevertheless, it is important to note that the overall spurious contributions to the macroscopic dynamics can be expected to be diluted due to the pre-multipliers to these error terms.

To illustrate this, we consider the guided equilibrium distribution representation [13–15]:

$$f_i^{eq} = \rho \prod_{\alpha=x,y} \frac{(1 - 2c_{i_\alpha}^2)}{2^{c_{i_\alpha}^2}} [c_{i_\alpha}^2 - 1 + c_{i_\alpha} u_\alpha + u_\alpha^2 + \theta], \quad (8)$$

that is defined for the D2Q9 lattice and for which $\Pi'_{\alpha\beta} = 0$ but $q'_\alpha \neq 0$. Using the guided equilibrium, we first evaluate Eq. (7) to obtain the non-equilibrium pressure tensor:

$$\Pi_{\alpha\beta}^{\text{OReg}} = -\mu_{\alpha\beta}^{\text{OReg}} \left(\partial_\alpha u_\beta + \partial_\beta u_\alpha - \partial_\chi u_\chi \delta_{\alpha\beta} \right) + (\Pi_{\alpha\beta}^{(neq)})' \quad (9a)$$

where,

$$\mu_{\alpha\beta}^{\text{OReg}} = \tau \rho \theta \begin{cases} \frac{1}{2\theta^2} (\theta - u_\alpha^2) (1 - \theta - u_\alpha^2) & \text{if } \alpha = \beta \\ 1 & \text{otherwise,} \end{cases} \quad (9b)$$

and,

$$(\Pi_{\alpha\beta}^{(neq)})' = \begin{cases} 0 & \text{if } \alpha = \beta \\ \rho \frac{\tau}{2\theta} u_x u_y (u_x^2 - u_y^2) (\partial_x u_x - \partial_y u_y) & \text{otherwise.} \end{cases} \quad (9c)$$

It can be seen from Eq. (9c) that the diagonal components of the non-equilibrium pressure tensor are error-free while the off-diagonal components have an $\mathcal{O}(u^6)$ error. Thus, the contribution of $(\Pi_{\alpha\beta}^{(neq)})'$ to $\Pi_{\alpha\beta}^{\text{OReg}}$ is negligible and can be safely ignored. Now, with a vanishing $(\Pi_{\alpha\beta}^{(neq)})'$, Eq. (9a) explicitly yields a traceless $\Pi_{\alpha\beta}^{\text{OReg}}$ with a dynamic viscosity of $\mu_{\alpha\beta}^{\text{OReg}}$ which, as shown in

Eq. (9b), demonstrates that the OReg scheme intrinsically modifies the lattice viscosity of the diagonal components of $\Pi_{\alpha\beta}^{\text{OReg}}$ to compensate for the insufficient lattice isotropy of the D2Q9 lattice.

Next, we evaluate Eqs. (6a) and (6b) using the guided equilibrium to obtain:

$$\langle f_i^{\text{OReg}}, 1 \rangle = 0, \quad (10a)$$

$$\langle f_i^{\text{OReg}}, c_{i_\alpha} \rangle = \frac{\tau \rho u_\alpha}{\theta} (u_\alpha^2 + 3\theta - 1) \left(\partial_\alpha u_\alpha - \frac{1}{2} \partial_\chi u_\chi \right). \quad (10b)$$

It can be seen that, with the OReg scheme and the guided equilibrium, Eq. (10a) vanishes as required by the compatibility conditions; in contrast, Eq. (10b) is non-zero with a magnitude of $\mathcal{O}(u^5)$ and $\mathcal{O}(u^3)$ for $\theta = 1/3$ and $\theta \neq 1/3$, respectively. Consequently, due to the $(1/2\tau)$ factor in Eqs. (5a) and (5b), the corresponding mass and momentum conservation equations contain $\mathcal{O}(u^4)/\mathcal{O}(u^2)$ errors depending on the value of the isothermal temperature. Thus, with the OReg scheme and the guided equilibrium, one can conduct correction-free isothermal Navier-Stokes simulations with $\mathcal{O}(u^3)/\mathcal{O}(u)$ accuracy at the lattice reference temperature and arbitrary lattice temperatures, respectively.

We now proceed to numerically verify the theoretical results presented above. In order to obtain a fully local scheme, the derivative terms appearing in Eq. (3) are locally evaluated by using the definition of the second-order trace-free stress tensor [18–20] to generically represent the OReg populations as:

$$f_i^{\text{OReg}} = \frac{f_i^{(eq)}}{2\rho\theta^2} \left(C_{i_\alpha} C_{i_\beta} - \frac{C_i^2}{D} \delta_{\alpha\beta} \right) - \sum_{k=1}^N \left(c_{k_\alpha} c_{k_\beta} - \frac{c_k^2}{D} \delta_{\alpha\beta} \right) f_k^{(neq)}. \quad (11)$$

Note that, the presence of $f_i^{(neq)}$ in Eq. (11) allows the OReg scheme to be interpreted as a one-step predictor-corrector method where the prediction $f_i^{(1)} \approx f_i^{(neq)}$ is corrected to $f_i^{(1)} = f_i^{\text{OReg}}$. The predictor $f_i^{(neq)}$ can be evaluated through any existing regularization scheme [20]; however, for the sake of simplicity we use the naive representation of $f_i^{(neq)} = (f_i - f_i^{(eq)})$.

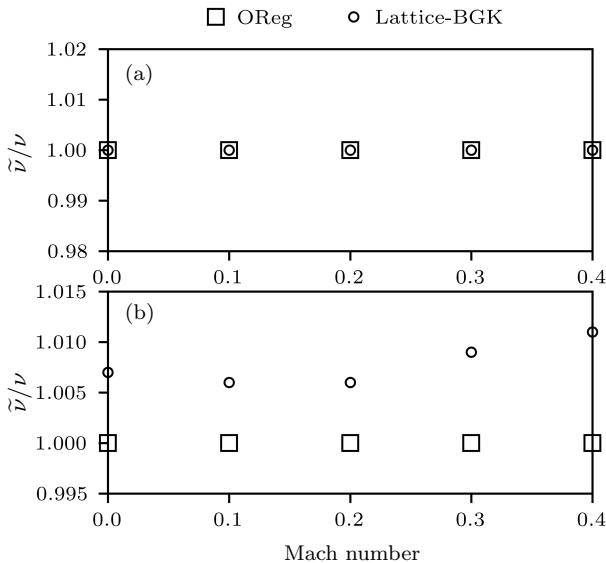


FIG. 2. Comparison of the numerically computed and physically imposed fluid viscosities, $\tilde{\nu}$ and ν , for a decaying shear wave at different Mach numbers obtained with the OReg and lattice-BGK schemes using the guided equilibrium (Eq. (8)) on the D2Q9 lattice. For the axis-aligned shear wave (panel (a)) both schemes correctly model the viscous dissipation as demonstrated by $\tilde{\nu}/\nu = 1$ while for the $\pi/4$ rotated wave (panel (b)) only the OReg scheme recovers the imposed viscous dissipation rate.

We first consider the classical linear benchmark case of a decaying shear wave [12, 15, 17]. In the absence of any spurious numerical errors, observed statistics for waves described by a wave vector $\mathbf{k} = m\hat{e}_{\parallel} + n\hat{e}_{\perp}$, where \hat{e}_{\parallel} and \hat{e}_{\perp} are unit vectors parallel and perpendicular to the wave, theoretically display an exponential time decay. Here we take the amplitude of the x -velocity component, $u_x^{max}(t)$, as the statistic of interest and compute the numerical kinematic viscosity, $\tilde{\nu}$, through the following curve fitting expression: $u_x^{max}(t) \propto \exp(-|\mathbf{k}|^2 \tilde{\nu} t)$. We consider two situations, namely an axis-aligned and a $\pi/4$ -rotated wave, respectively. Both cases are initialized with a unit density. The initial velocity field for the axis-aligned case is given as:

$$u_x = A_0 \sin\left(\frac{2\pi y}{L_y}\right), u_y = \text{Ma}\sqrt{\theta}, \quad (12a)$$

and that for the rotated wave case is given as:

$$u_x = A_0 \sin\left(\frac{2\pi}{L_y\sqrt{2}}(-x+y)\right), \quad (12b)$$

$$u_y = \text{Ma}\sqrt{\theta} + A_0 \sin\left(\frac{2\pi}{L_y\sqrt{2}}(-x+y)\right).$$

The wave vectors for the two cases are $\frac{2\pi}{L_y}\hat{j}$ and $\frac{\pi}{L_y}(-\hat{i}+\hat{j})$ respectively. The values of the wave amplitude (A_0) and spatial discretization in the y -direction (L_y) are taken to be 0.001 and 200 respectively. Simulations are conducted using the lattice-BGK and OReg schemes at the reference

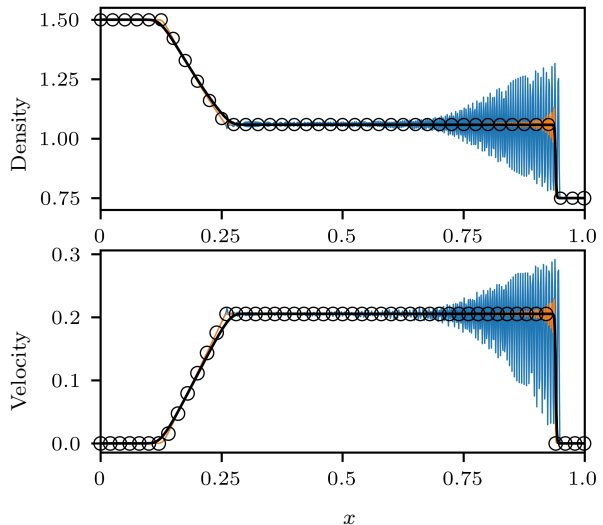


FIG. 3. Isothermal shocktube results ($\theta = 0.35$, $\nu = 10^{-5}$) using the guided equilibrium (Eq. (8)) on the D2Q9 lattice. The solid blue and orange curves correspond to the lattice-BGK and the third order Essentially Entropic LB respectively whereas the solid black curve corresponds to the OReg scheme. The round black symbols correspond to the analytical solution.

temperature $\theta = 1/3$ with an imposed kinematic viscosity $\nu = 0.01$ for different Mach numbers.

In the axis-aligned case, the spurious errors due to lattice anisotropy are dormant and consequently the lattice-BGK recovers the correct dissipation rate [15] as shown in Fig. 2(a); it can be seen that the OReg scheme also recovers the correct dissipation rate. For the rotated wave case, the spurious contributions are activated and, as shown in Fig. 2(b), the uncorrected lattice-BGK model fails to recover the dissipation accurately. In contrast, the OReg scheme yields the accurate dissipation rate without having to incorporate any correction terms.

The second benchmark we consider is that of a one-dimensional shocktube operating at appreciably small viscosities and lattice temperatures of $\theta \neq 1/3$. It has been previously shown that the OReg scheme, used with an $\mathcal{O}(u^4)$ polynomial equilibrium representation, exactly recovers the analytical solution in an athermal setting where $\theta = 1/3$ for a lattice viscosity $\nu = 10^{-7}$ [19]. Here, we examine the behaviour of the OReg scheme with the guided equilibrium when employed at elevated operating temperatures and lattice viscosities of $\theta = 0.35$, $\nu = 10^{-5}$ and $\theta = 0.4$, $\nu = 10^{-9}$, respectively.

In Figs. (3), (4), we present the numerical results obtained from the lattice-BGK, the state-of-the-art third-order Essentially Entropic LB (EELB) [29], and the OReg scheme, along with comparisons against analytical solutions. The simulation is run on a 800×1 grid for 500 timesteps and employs the second order halfway bounce-back treatment for the walls. It can be seen that while the lattice-BGK yields the largest oscillations and the EELB significantly reduces those oscillations, the OReg scheme

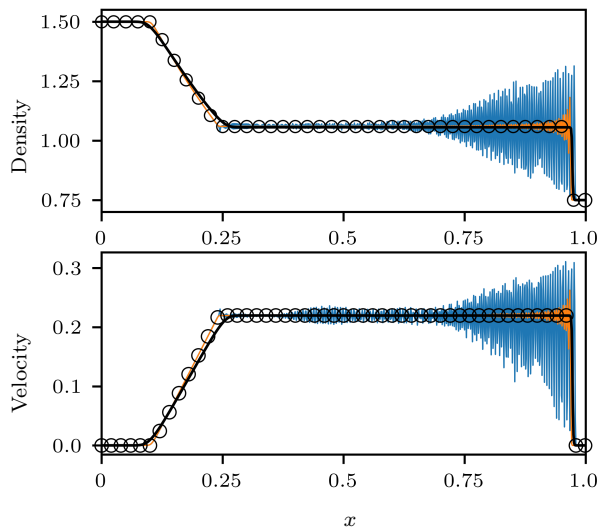


FIG. 4. Isothermal shocktube results ($\theta = 2/5$, $\nu = 10^{-9}$) using the guided equilibrium (Eq. (8)) on the D2Q9 lattice. The curves have the same meaning as in 3.

completely eliminates them. Note that the OReg scheme yields a slightly incorrect slope in the high-density region due to the first-order nature of the resulting hydrodynamics at temperatures of $\theta \neq 1/3$. However, a computation of the L_2 errors reveals that the OReg scheme captures the density with an accuracy of approximately 98.88% and 98.20% respectively. The simulations conducted on grids of halved and doubled grids also yield similar accuracy indicating grid independence of the solution. Lastly, it is noteworthy that while the accuracy of the EELBM scheme improves with increasing grid size, it still retains spurious oscillations; in contrast even on halved grids, the OReg scheme eliminates the spurious oscillations.

In conclusion, we have shown that the OReg scheme yields stable and accurate results on computationally efficient first-neighbour lattices, coping with the long-standing limitations induced by the anisotropy error, which have been plaguing LB simulations so far. Specifically, with the guided equilibrium defined on the D2Q9 lattice, the OReg scheme is shown to recover isothermal hydrodynamics with third-order accuracy for simulations conducted at the lattice reference temperature and with first-order accuracy at arbitrary lattice temperatures. Recall that the guided equilibrium is not fully constrained as Eq. (8) does not recover the equilibrium heat flux vector Eq. (1c); indeed, the deviations in $Q'_{\alpha\beta\gamma}$ and $R'_{\alpha\beta\gamma\mu}$ for a fully constrained equilibrium representation, may yield a more accurate model for isothermal temperatures of $\theta \neq 1/3$. Nevertheless, even in the current form, the OReg scheme can be coupled to a second population to conduct fully local thermal and compressible flow simulations on standard lattices. We also highlight that the OReg scheme presented in Eq. (11) is generic and can be seamlessly generalized to any lattice

stencil. Indeed, with appropriate equilibrium representations, the OReg scheme can be directly integrated into high-performance codes such as, e.g., waLBerla [30] and highly optimized GPU implementations [31, 32]. Further, the OReg scheme also presents a promising alternative to locally defining the so-Grad boundary conditions [33, 34]. Thus, the OReg scheme presents a significant advance for conducting scalable simulations of physically relevant non-linear dissipative transport problems (see, e.g., [35]) characterized by multiscale phenomena possibly in complex geometries. Studies exploring these avenues will be the subject of future work.

The authors would like to thank Prof. I.V. Karlin and Dr. Syed Ali Hosseini for their valuable comments during the preparation of this manuscript.

* Corresponding author: anirudh.jonnalagadda@iit.it

- [1] R. Benzi, S. Succi, and M. Vergassola, The lattice boltzmann equation: theory and applications, *Physics Reports* **222**, 145 (1992).
- [2] S. Chen and G. D. Doolen, Lattice boltzmann method for fluid flows, *Annual review of fluid mechanics* **30**, 329 (1998).
- [3] C. K. Aidun and J. R. Clausen, Lattice-boltzmann method for complex flows, *Annual review of fluid mechanics* **42**, 439 (2010).
- [4] A. Tiribocchi, M. Durve, M. Lauricella, A. Montessori, J.-M. Tucny, and S. Succi, Lattice boltzmann simulations for soft flowing matter, *Physics Reports* **1105**, 1 (2025).
- [5] Y. Chen, H. Ohashi, and M. Akiyama, Thermal lattice bhatnagar-gross-krook model without nonlinear deviations in macrodynamic equations, *Phys. Rev. E* **50**, 2776 (1994).
- [6] A. J. Wagner and J. M. Yeomans, Phase separation under shear in two-dimensional binary fluids, *Phys. Rev. E* **59**, 4366 (1999).
- [7] P. J. Dellar, Nonhydrodynamic modes and a priori construction of shallow water lattice boltzmann equations, *Phys. Rev. E* **65**, 036309 (2002).
- [8] P. J. Dellar, Incompressible limits of lattice boltzmann equations using multiple relaxation times, *Journal of Computational Physics* **190**, 351 (2003).
- [9] G. Hazi and P. Kavran, On the cubic velocity deviations in lattice boltzmann methods, *Journal of Physics A: Mathematical and General* **39**, 3127 (2006).
- [10] G. Hazi and C. Jimenez, Simulation of two-dimensional decaying turbulence using the “incompressible” extensions of the lattice boltzmann method, *Computers & Fluids* **35**, 280 (2006).
- [11] B. Keating, G. Vahala, J. Yopez, M. Soe, and L. Vahala, Entropic lattice boltzmann representations required to recover navier-stokes flows, *Phys. Rev. E* **75**, 036712 (2007).
- [12] P. J. Dellar, Lattice boltzmann algorithms without cubic defects in galilean invariance on standard lattices, *Journal of Computational Physics* **259**, 270 (2014).
- [13] N. I. Prasianakis and I. V. Karlin, Lattice boltzmann method for thermal flow simulation on standard lattices,

- Phys. Rev. E **76**, 016702 (2007).
- [14] N. I. Prasianakis and I. V. Karlin, Lattice boltzmann method for simulation of compressible flows on standard lattices, Phys. Rev. E **78**, 016704 (2008).
- [15] N. I. Prasianakis, I. V. Karlin, J. Mantzaras, and K. B. Boulouchos, Lattice boltzmann method with restored galilean invariance, Phys. Rev. E **79**, 066702 (2009).
- [16] M. H. Saadat, F. Bösch, and I. V. Karlin, Lattice boltzmann model for compressible flows on standard lattices: Variable prandtl number and adiabatic exponent, Phys. Rev. E **99**, 013306 (2019).
- [17] M. H. Saadat, B. Dorschner, and I. Karlin, Extended lattice boltzmann model, Entropy **23**, 10.3390/e23040475 (2021).
- [18] A. Jonnalagadda, A. Sharma, and A. Agrawal, Revisiting the Lattice Boltzmann Method Through a Nonequilibrium Thermodynamics Perspective, Journal of Heat Transfer **143** (2021), 052102.
- [19] A. Jonnalagadda, A. Sharma, and A. Agrawal, Onsager-regularized lattice boltzmann method: A nonequilibrium thermodynamics-based regularized lattice boltzmann method, Phys. Rev. E **104**, 015313 (2021).
- [20] A. Jonnalagadda, A. Sharma, and A. Agrawal, On application of the regularized lattice boltzmann method for isothermal flows with non-vanishing knudsen numbers, Numerical Heat Transfer, Part B: Fundamentals **84**, 756 (2023).
- [21] S. Hosseini, M. Atif, S. Ansumali, and I. Karlin, Entropic lattice boltzmann methods: A review, Computers & Fluids **259**, 105884 (2023).
- [22] A. K. Mahendra, *Meshless method for Slip flows*, Ph.D. thesis, Homi Bhabha National Institute (2011).
- [23] A. K. Mahendra and R. K. Singh, Onsager reciprocity principle for kinetic models and kinetic schemes (2013), arXiv:1308.4119 [physics.flu-dyn].
- [24] L. Onsager, Reciprocal relations in irreversible processes. i., Phys. Rev. **37**, 405 (1931).
- [25] L. Onsager, Reciprocal relations in irreversible processes. ii., Phys. Rev. **38**, 2265 (1931).
- [26] S. Chapman and T. Cowling, *The mathematical theory of non-uniform gases*, 3rd ed. (Cambridge : Cambridge University Press, 1970).
- [27] S. Succi, *The lattice Boltzmann equation: for fluid dynamics and beyond* (Oxford university press, 2001).
- [28] T. Krüger, Halim Kusumaatmaja, Alexandr Kuzmin, Or-est Shardt, Goncalo Silva, and Erlend Mahnus Viggen, *The Lattice Boltzmann Method: Principles and Practice*, 1st ed. (Springer International Publishing, 2017).
- [29] M. Atif, P. K. Kolluru, C. Thantapanally, and S. Ansumali, Essentially entropic lattice boltzmann model, Phys. Rev. Lett. **119**, 240602 (2017).
- [30] M. Bauer, S. Eibl, C. Godenschwager, N. Kohl, M. Kuron, C. Rettinger, F. Schornbaum, C. Schwarzeimer, D. Thönnies, H. Köstler, and U. Rüde, walberla: A block-structured high-performance framework for multiphysics simulations, Computers & Mathematics with Applications **81**, 478 (2021), development and Application of Open-source Software for Problems with Numerical PDEs.
- [31] A. Montessori, M. La Rocca, G. Amati, M. Lauricella, A. Tiribocchi, and S. Succi, High-order thread-safe lattice boltzmann model for high performance computing turbulent flow simulations, Physics of Fluids **36**, 035171 (2024).
- [32] M. Lauricella, A. Tiribocchi, S. Succi, L. Brandt, A. Mukherjee, M. L. Rocca, and A. Montessori, Thread-safe multiphase lattice boltzmann model for droplet and bubble dynamics at high density and viscosity contrasts (2025), arXiv:2501.00846 [physics.flu-dyn].
- [33] J. Latt, B. Chopard, O. Malaspinas, M. Deville, and A. Michler, Straight velocity boundaries in the lattice boltzmann method, Phys. Rev. E **77**, 056703 (2008).
- [34] B. Dorschner, S. Chikatamarla, F. Bösch, and I. Karlin, Grad's approximation for moving and stationary walls in entropic lattice boltzmann simulations, Journal of Computational Physics **295**, 340 (2015).
- [35] I. Rasin, W. Miller, and S. Succi, Phase-field lattice kinetic scheme for the numerical simulation of dendritic growth, Phys. Rev. E **72**, 066705 (2005).